Solvent Exfoliation of Transition Metal Dichalcogenides: Dispersibility of Exfoliated Nanosheets Varies Only Weakly between Compounds

Graeme Cunningham,[†] Mustafa Lotya,[†] Clotilde S. Cucinotta,[†] Stefano Sanvito,[†] Shane D. Bergin,[‡] Robert Menzel,[‡] Milo S. P. Shaffer,[‡] and Jonathan N. Coleman[†,*]

[†]School of Physics and CRANN, Trinity College Dublin, Dublin 2, Ireland, and [‡]Department of Chemistry, Imperial College London, South Kensington Campus, London SW7 2AZ, United Kingdom

ABSTRACT We have studied the dispersion and exfoliation of four inorganic layered compounds, WS_2, MoS_2, $MoSe_2$, and $MoTe_2$, in a range of organic solvents. The aim was to explore the relationship between the chemical structure of the exfoliated nanosheets and their dispersibility. Sonication of the layered compounds in solvents generally gave few-layer nanosheets with lateral dimensions of a few hundred nanometers. However, the dispersed concentration varied greatly from solvent to solvent. For all four materials, the concentration peaked for solvents with surface energy close to 70 mJ/m^2, implying that all four have surface energy close to this value. Inverse gas chromatography measurements showed MoS_2 and $MoSe_2$ to have surface energies of ~75 mJ/m^2, in good agreement with dispersibility measurements. However, this method suggested $MoTe_2$ to have a considerably larger surface energy (~120 mJ/m^2). While surface-energy-based solubility parameters are perhaps more intuitive for two-dimensional materials, Hansen solubility parameters are probably more useful. Our analysis shows the dispersed concentration of all four layered materials to show well-defined peaks when plotted as a function of Hansen's dispersive, polar, and H-bonding solubility parameters. This suggests that we can associate Hansen solubility parameters of $\delta_D \sim 18$ MPa$^{1/2}$, $\delta_P \sim 8.5$ MPa$^{1/2}$, and $\delta_H \sim 7$ MPa$^{1/2}$ with all four types of layered material. Knowledge of these properties allows the estimation of the Flory–Huggins parameter, χ, for each combination of nanosheet and solvent. We found that the dispersed concentration of each material falls exponentially with χ as predicted by solution thermodynamics. This work shows that solution thermodynamics and specifically solubility parameter analysis can be used as a framework to understand the dispersion of two-dimensional materials. Finally, we note that in good solvents, such as cyclohexylpyrrolidone, the dispersions are temporally stable with >90% of material remaining dispersed after 100 h.

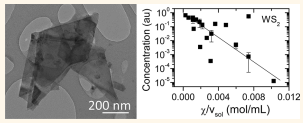

KEYWORDS: solvent exfoliation · dispersibility · dichalcogenide

Over the past decade, two-dimensional nanomaterials have become one of the most studied subfields of nanoscience. These developments have been spearheaded by research into graphene, a material that is unique due to its combination of thermal, electronic, optical, and mechanical properties.[1−5] However, over the past few years, it has become clear that a range of other inorganic layered compounds can be mechanically exfoliated in small quantities to give two-dimensional nanosheets with interesting properties.[6−10] For example, exfoliated hexagonal boron nitride has been used as a dielectric support in graphene-based transistors[11] while MoS_2 has been fabricated into sensors,[10,12] transistors,[13−15] and integrated circuits.[16] The availability of a wide range of two-dimensional materials is important as it allows access to a broad palette of physical and chemical properties. A good example is provided by the family of transition metal dichalcogenides (TMDs). These materials have the chemical composition MX_2, where M is a transition metal (commonly, but not limited to Ti, Nb, Ta, Mo, W) and X is a chalcogen (*e.g.*, S, Se, Te). As in graphite, these atoms are covalently bonded into nanosheets which stack into three-dimensional crystals by van der Waals interactions. These materials are of particular interest because, depending on the combination of metal and chalcogen, the material can be semiconducting or metallic.[17] In addition, the band gap can vary from a few hundred millielectronvolts to a few electronvolts,[17] suggesting these materials have potential as versatile electronic device materials. Furthermore, these materials have interesting electrochemical properties which make them suitable for applications such as battery electrodes.[18,19]

As with graphene, many applications will require relatively large quantities of material, suggesting that a solution processing route is required.[20] A number of possibilities exist. For example, it has been known for many years that materials such as MoS_2 can be exfoliated by lithium intercalation.[21] Unfortunately, such a route tends to result in

* Address correspondence to colemaj@tcd.ie.

Received for review February 3, 2012 and accepted March 6, 2012.

Published online March 06, 2012
10.1021/nn300503e

structural deformations in some TMDs, leading to considerably altered electronic properties.[22] Alternatively, TMDs can be synthesized in the liquid phase.[7,8] However, the simplest route to liquid exfoliation of layered compounds is sonication-assisted exfoliation in solvents[23−29] or aqueous surfactant solutions.[19,30−32] Here, sonication results in the exfoliation of the layered crystal into single and multilayer nanosheets which are then stabilized by interaction with the solvent or a surfactant. This method has the advantage of extreme simplicity coupled with the fact that it results in small but high-quality exfoliated nanosheets which can then be fabricated into films or composite materials.[19,23]

Solvent exfoliation is probably the most practical approach due to its simplicity and the lack of a third-phase dispersant (*i.e.*, a surfactant). However, very little is known about the stabilization mechanism. While detailed studies on solvent exfoliation of carbon nanotubes[33] and graphene[25] have been reported, no corresponding analysis has appeared for inorganic layered compounds. Such an analysis would be useful as a detailed insight into the exfoliation mechanism would allow both the optimization of the exfoliation process and the discovery of new solvents.

Any detailed study of solvent exfoliation of layered compounds must address a number of simple questions. Most fundamentally, it will be critical to know whether solution thermodynamics can be used as a framework to describe this process. If so, what solubility parameters can be used and which are most appropriate? While the surface energy has been used as a solubility parameter for carbon nanotubes and graphene, it is not clear whether this term is well-suited for other van der Waals bonded systems. If the surface energy is an appropriate solubility parameter, does the surface energy predicted from solubility measurements match that measured by other means? How do the surface energies, and so solvent requirements, depend on the nature of the nanosheet surface? It is critical that such questions be answered in order to develop the large-scale exfoliation of these materials further.

In this paper, we describe experiments to estimate the dispersibility of four different types of nanosheet in a wide range of solvents with the aim of answering these questions. We choose the layered materials (WS_2, MoS_2, $MoSe_2$, $MoTe_2$) to controllably vary the nature of the surface which interacts with the solvent. The results have been analyzed within the framework of solution thermodynamics. We believe that this study casts new light on the factors controlling the dispersibility of inorganic nanosheets in organic solvents.

RESULTS AND DISCUSSION

Characterization of Dispersions. We have measured the optical absorbance spectra of dispersions of WS_2, MoS_2, $MoSe_2$, and $MoTe_2$ exfoliated in 21 different solvents (see Methods). Typical spectra are shown in Figure 1A. As observed previously for MoS_2 and WS_2, these spectra appear to be superimposed on a power law background (inset).[23] Otherwise, the spectral shapes are as expected.[17] We use the absorbance divided by cell length at set wavelengths, A/l, as a semiquantitative measure of the dispersed concentration (subject to the provisos mentioned in Methods). The measured values are listed in Table S1 (Supporting Information) and show the dispersed concentration to vary by 3 orders of magnitude over the range of solvents used. We note that, for each material, the best solvent is either NMP or CHP, solvents which are also known to efficiently disperse carbon nanotubes and graphene.[25,33−37]

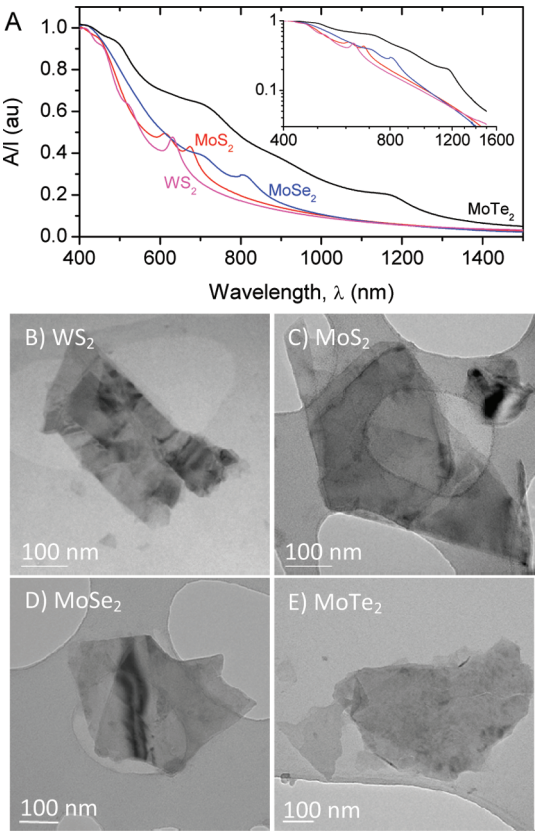

Figure 1. (A) Normalized absorbance spectra for dispersions of the four transition metal dichalcogenides in the solvent cyclohexylpyrrolidone (CHP). Inset: log−log plot suggests the presence of a power law scattering background. (B−E) Representative TEM images of multilayer nanosheets of each of the four TMDs.

We can assess the state of the dispersed material using TEM. Shown in Figure 1B−E are typical images of flakes observed in the CHP dispersions. In all cases, stacked multilayer nanosheets were found, with no evidence of individual nanosheets. Although it is as yet impossible to unambiguously identify individual nanosheets, in a previous study we produced what we believe to be monolayers using smaller sonic baths.[23] We attribute the lack of monolayers observed here to the sonication scheme used. We used a large volume,

low power density bath which was chosen for its throughput rather than its suitability for high-quality exfoliation. This study involved the preparation of ~250 dispersions, a quantity which would be completely unmanageable using the small sonic baths which tend to give highly exfoliated flakes.[23,36] The difference in sonication schemes between this work and our previous report[23] may result in some slight variation in the relative performance of solvents. However, even though the exfoliation is not optimized here, it is probable that the relative concentrations of the dispersions are controlled by the solvent–nanosheet interaction. However, due to the fact that the sonication scheme is suboptimal, we should expect considerable scatter in the data. The flakes were typically a few hundred nanometers in length, in agreement with previous work.[23]

We further analyzed the dispersed material by filtering the dispersions through porous membranes to form thin films. SEM images of these films are shown in Figure 2A–D. These images show large quantities of 2D objects arranged in a disordered network. We have observed no evidence of significant quantities of three-dimensional material. We have also characterized these films by Raman spectroscopy, as shown in Figure 3E (λ_{ex} = 514 nm). In each case, a number of well-defined peaks are observed in the region of 150–450 cm^{-1}. It is known from the literature that such peaks can be used to identify layered compounds.[38–40] We have marked the expected positions[38–40] of the dominant bands for each material in Figure 3E. In each case, these positions match reasonably well to the observed peaks. We note that the literature positions are for stacked crystals. It is well-known that shifts of a few wavenumbers occur on exfoliation,[6] leading to the slight disagreement between measured and predicted peak positions.

Role of Surface Energy. Once it has been confirmed that the dispersed material consists predominately of exfoliated few-layer nanosheets, one can consider the mechanism for dispersion and exfoliation. For non-electrolytic systems, mixing of solvent and solute is generally understood *via* the free energy of mixing, ΔG_{Mix}.[41] This quantity represents the difference in free energy between a mixture of two components and the two components in their unmixed form and is usually written as

$$\Delta G_{Mix} = \Delta H_{Mix} - T\Delta S_{Mix} \quad (1)$$

where ΔH_{Mix} is the enthalpy of mixing and ΔS_{Mix} is the entropy of mixing. If ΔG_{Mix} is negative, mixing is favorable. For mixtures of large solutes such as nanosheets, ΔS_{Mix} can be very small. This means that for mixing to occur ΔH_{Mix} should be as low as possible, making it important to understand the factors which control ΔH_{Mix}. Because the exfoliated material is two-dimensional with lateral size typically of hundreds of nanometers, we can assume that the solvent–nanosheet interaction occurs primarily at the basal plane surface. Some time ago, we developed a model to study the balance of van der Waals interactions under such circumstances.[34,36] This model predicts the enthalpy of mixing, ΔH_{Mix}, per volume of mixture, V, of a nanosheets dispersion to be[36]

$$\frac{\Delta H_{Mix}}{V} \approx \frac{2}{T_{NS}}(\sqrt{\gamma_S} - \sqrt{\gamma_{NS}})^2\phi \quad (2)$$

where γ_S and γ_{NS} are the total surface energies of solvent and nanosheet, respectively, T_{NS} is the nanosheet thickness, and ϕ is the dispersed nanosheet volume fraction (proportional to the concentration, C; $C = \rho\phi$, where ρ is the nanosheet density). This expression predicts that the energetic cost of dispersing the nanosheets is minimized for solvents with surface energy very close to that of the nanosheet. One would

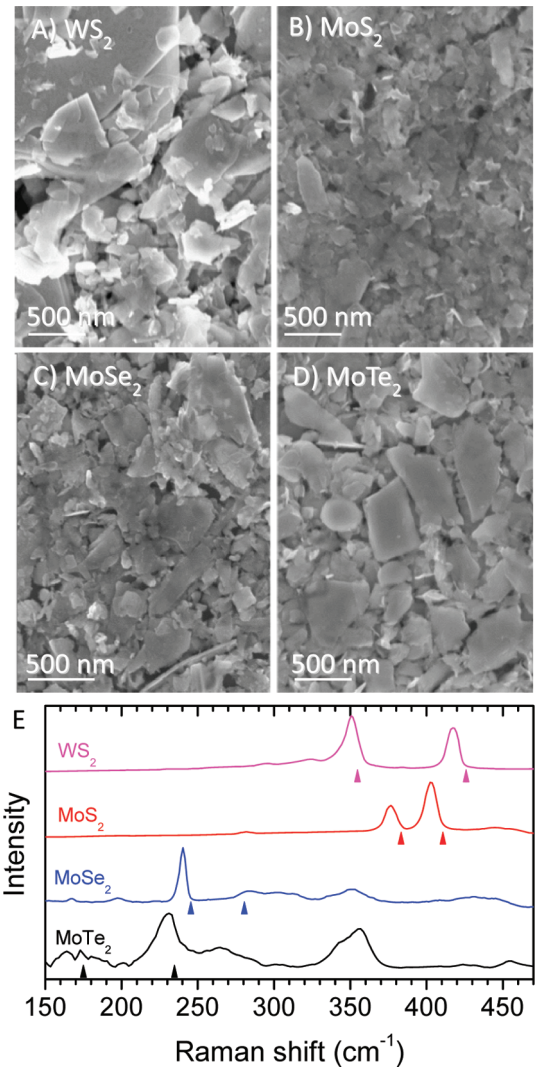

Figure 2. (A–D) SEM images of the surface of thin vacuum filtered films of each of the four transition metal dichalcogenides used in this study. (E) Raman spectra (λ_{ex} = 532 nm) of each of the films shown above. The arrows mark the positions of the main lines observed for stacked crystals of each material.

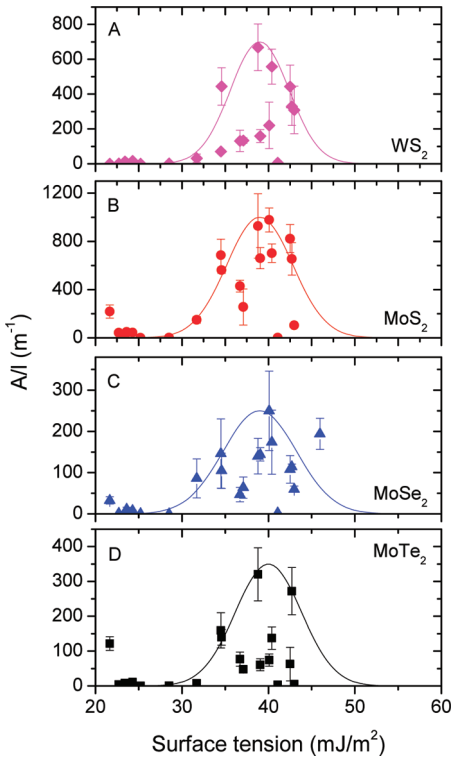

Figure 3. Absorbance per cell length (proportional to dispersed concentration) for each transition metal dichalcogenide dispersed in a range of solvents plotted as a function of solvent surface tension. The lines represent Gaussian envelope functions.

expect such solvents to give the maximum dispersed concentration. We can make this prediction quantitative using recent work which has shown that for rod-like solutes the maximum dispersed volume fraction is given by[42]

$$\phi \propto \exp\left[-\frac{\bar{v}}{RT} \frac{\partial(\Delta H_{Mix}/V)}{\partial \phi} \right] \quad (3)$$

where $\bar{v}$ is the volume per mole of the dispersed phase and T is the absolute temperature. Assuming we can model a nanosheet as a very low aspect ratio cylinder, we can insert eq 2 into eq 3 to yield

$$\phi \propto \exp\left[-\frac{\pi D_{NS}^2}{2kT} (\sqrt{\gamma_S} - \sqrt{\gamma_{NS}})^2 \right] \quad (4)$$

where D_{NS} is the nanosheet diameter (modeling it as a disk). We can simplify this expression by using the approximation $(x - a)^2 \approx 4a(\sqrt{x} - \sqrt{a})^2$, which is reasonably accurate so long as the full width at half-maximum of the resulting Gaussian is less than about half the center value. In this work, we are always well within these limits. Applying this approximation and expressing in terms of dispersed concentration gives

$$C \propto \exp\left[-\frac{\pi D_{NS}^2}{8\gamma_{NS}kT} (\gamma_S - \gamma_{NS})^2 \right] \quad (5)$$

This equation predicts that the dispersed concentration should display a Gaussian-shaped peak when plotted as a function of solvent surface energy. (In practice, we work in terms of solvent surface tension, Γ, which is linked to surface energy, γ, by $\Gamma = \gamma_S - TS_S$, where S_S is the surface entropy and $TS_S \approx 29$ mJ/m^2 for almost all liquids at room temperature.)[43,44] Graphs of the dispersed concentration of each TMD as a function of solvent surface tension are shown in Figure 3. Although the data are quite scattered, we find that appreciable amounts of material are only dispersed for surface tensions ~40 mJ/m^2. The position of this peak implies that $\gamma_{NS} \sim 70$ mJ/m^2, very similar to what is observed for carbon nanotubes, graphene, and hexagonal boron nitride.[23,33,34,45] For each material, we have manually fitted a Gaussian envelope function. We note that, as is usually the case,[25,33] many solvents give dispersed concentrations significantly below the envelope. The possible reasons for this variation will be discussed below.

We note that, by inspection of eq 5, we see that the full widths at half-max (fwhm) of the envelope functions in Figure 3 are related to the nanosheet diameter by

$$\text{fwhm} = \frac{1.6}{D_{NS}} \sqrt{\frac{8\gamma_{NS}kT}{\pi}} \quad (6)$$

The widths of the envelope functions in Figure 3 are in the range of 8−10 mJ/m^2. Using eq 6, we can use this value to estimate $D_{NS} \sim 5$ nm. This estimate is clearly approximately 2 orders of magnitude smaller than the flakes observed in the TEM and SEM images. Indeed, for flakes larger than 100 nm, the fwhm should be less than 1 mJ/m^2. The magnitude of the variation is similar to that found when applying this model to carbon nanotube dispersions.[42] The mechanism for broadening is currently unknown. However, the discrepancy certainly suggests that the analysis used here, while a useful guide, does not fully describe the interactions between solvents and nanostructures.

In addition, we must point out a shortcoming in our data sets. There are actually a relatively small number of solvents with surface tension above 45 mJ/m^2. This limitation means that it is impossible to populate the right-hand side of the graphs in Figure 3 to a level that would unambiguously show the fall off of concentration at high surface tension. This problem arises particularly for data with significant scatter and so applies specifically to the data for $MoTe_2$. It is, therefore, impossible to be absolutely certain of either the position or width of the Gaussian envelope function for this material.

Nevertheless, we note that the analysis above suggests two important points. The first is that the surface energies of these layered compounds appear to be relatively similar within the limitations imposed by the number of available solvents. This similarity suggests that the surface energy and presumably the strength of interactions between TMD nanosheets and adjacent

molecules depends only weakly on the identity of either the chalcogenide or the transition metal. This invariance of surface energy with chemical structure is an interesting result that can be linked to fundamental physics of intermolecular interactions. For extended objects (consisting of only one atomic species for simplicity) interacting by London interactions, the interaction strength is always proportional to $\alpha^2 N_V^2$, where α is the atomic polarizability and N_V is the atomic number density.[46] However, because α scales approximately with the atomic volume, αN_V is roughly constant and so approximately independent of the material in question. Obviously, this is a gross oversimplification, which is less relevant to more complex materials such as TMDs. However, it does show that it is plausible that such chemically dissimilar materials such as graphene, BN, and TMDs have similar surface energies and so can be dispersed in similar solvents.

The second important point is that the surface energy of all four layered compounds is close to 70 mJ/m^2. As mentioned above, this value is similar to that found for other materials which interact through van der Waals interactions. However, such values are in conflict with the published values of surface energy of several hundred millijoules per square meter for TMDs.[47,48] These values were calculated by computation some years ago, and we have been unable to find experimentally measured values to benchmark our results against. There is a significant possibility that these published values are simply too high. Indeed, such high values would suggest liquid exfoliation to be unlikely and may explain why so much effort was devoted to alternative exfoliation techniques such as ion intercalation.

Measurement of Surface Energy by Inverse Gas Chromatography. Given the important role played by surface energy in the exfoliation of layered materials, we believe it essential to have a good estimate of the actual surface energy of such materials. To this end, we characterized MoS_2, $MoSe_2$, and $MoTe_2$ by inverse gas chromatography (IGC), an analytical technique based on the retention of well-defined organic vapors by a packed powder bed of the solid. Note that WS_2 was excluded from the IGC studies as liquid nitrogen adsorption measurements (Supporting Information) indicated a significant fraction of micropores for this material, rendering IGC data analysis and interpretation challenging.

We note that IGC is most suited to the measurement of the dispersive component of the surface energy γ_D (*i.e.*, the intrinsic surface energy of the solid related to Lifshitz–van der Waals or London interactions). To measure γ_D, the net retention times of a series of *n*-alkanes were measured for each chalcogenide and the corresponding net retention volumes, V_n, calculated. According to a well-established model introduced by Schultz and co-workers, V_n is correlated

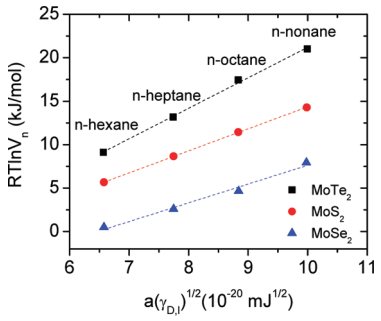

Figure 4. Inverse gas chromatographic characterization of MoS_2, $MoSe_2$, and $MoTe_2$. Plots of the net retention volumes, V_n, of four *n*-alkane adsorbates *versus* the adsorbates' molecular cross sections, *a*, and dispersive liquid tension, $\gamma_{D,l}$, according to Schultz (eq 7). The slopes of the three regression lines are proportional to the square root of dispersive surface energies, γ_D, of the three layered materials.

TABLE 1. Surface Energies of MoS_2, $MoSe_2$, and $MoTe_2$, As Determined by IGC: Dispersive Surface Energies, γ^d, and Specific Interaction Parameters, I_{sp}, of Selected Polar Adsorbates

TMD	γ_D [mJ/m^2]	I_{sp} (ethyl acetate) [mJ/m^2]	I_{sp} (1-propanol) [mJ/m^2]
MoS_2	44	18	30
$MoSe_2$	40	30	42
$MoTe_2$	84	21	34

to γ_D by[49]

$$RT\ln V_n = 2N_A(\gamma_D)^{1/2}a(\gamma_{D,l})^{1/2} + C \qquad (7)$$

where $\gamma_{D,l}$ is the dispersive surface free energy of the adsorbate in the liquid phase, *a* the molecular cross section of the adsorbate, N_A Avogadro's number, and *C* a general integration constant. Hence, γ_D can be determined by plotting $RT\ln V_n$ *versus* $a(\gamma_{D,l})^{1/2}$ for a series of *n*-alkanes, as shown in Figure 4. For all three materials studied, good regression coefficients ($r^2 >$ 0.98) were obtained over the range of the four *n*-alkane adsorbates, indicating robustness of the obtained data. For MoS_2 and $MoSe_2$, the dispersive surface energies derived from the slopes in Figure 4 were very similar at approximately 40 mJ/m^2 (Table 1). However, for $MoTe_2$, the IGC data indicated a significantly higher dispersive surface energy of 84 mJ/m^2.

Compared to other materials characterized by IGC, all three chalcogenides have dispersive surface energies which are similar to fullerenes (γ_D = 20–60 mJ/m^2).[50] However, they are larger than conventional organic polymers (*e.g.*, poly(methyl methacrylate), γ_D = 30–35 mJ/m^2)[51] but significantly lower than purely graphitic surfaces (*e.g.*, graphite, γ_D = 80–120 mJ/m^2; multiwalled carbon nanotubes, γ_D = 90–120 mJ/m^2).[51,74] However, it is worth noting that surface energy values as low as 55 mJ/m^2 have been measured for graphite by contact angle measurements,[52] while solubility measurements suggest a value closer to

70 mJ/m^2.[25,36] We note that graphitic surfaces are known to be highly heterogeneous, leading to wide variations in surface energy measurements and wetting hysteresis under different conditions.[50,52,53] Recent measurements quantifying the heterogeneity of carbon nanotube surfaces[75] highlighted this issue and suggest a promising future area for the study of 2D compounds. The difference in γ_D of $MoTe_2$ and MoS_2/$MoSe_2$ is consistent with the larger polarizability volume of tellurium (9.6 Å^3) compared to sulfur (7.3 Å^3) and selenium (7.5 Å^3), and the small difference in electronegativity in the Mo−Te bond (0.06) compared to the Mo−S and Mo−Se bonds (0.42 and 0.39, respectively).[54] Furthermore, our experimental IGC results agree qualitatively with recent theoretical calculations[55] which found $MoTe_2$ to have a larger surface energy than MoS_2 and $MoSe_2$.

It should be noted that the γ_D values presented in Table 1 do not include specific contributions, γ_{sp}, to the total surface energy, that is, solid surface energy components due to polar interactions, hydrogen bonding, or other nondispersive interactions. The determination of a numerical value for γ_{sp}, intrinsic to the solid surface, is very challenging. Experimental measurements based on various theoretical paradigms yield widely diverging γ_{sp} values, even for relatively well-studied solid surfaces, such as poly(methyl methacrylate) (PMMA).[56] However, IGC can be used to unambiguously measure the specific contribution to the free energy of adsorption, ΔG_{sp}, for a given polar adsorbate (in kJ/mol), determined as the difference of $RT\ln V_n$ of the polar probe to the corresponding dispersive reference line in Figure 4:[49]

$$\Delta G_{sp} = RT\ln V_n - RT\ln V_n^{ref} \quad (8)$$

Such ΔG_{sp} values can be harmonized with the units of the dispersive surface energy (mJ/m^2) using[57]

$$I_{sp} = \frac{\Delta G_{sp}}{aN_A} \quad (9)$$

where I_{sp} is the specific interaction parameter. Even though I_{sp} is not an intrinsic property of the solid surface (as it depends on the selected adsorbate), it can be considered a rough indicator for the order of magnitude of the specific solid surface energy. In order to estimate the potential of the layered materials to interact through nondispersive forces, we carried out IGC measurements with ethyl acetate (containing a functional ester group that can interact *via* polar interactions) and 1-propanol (containing a hydroxyl group that can interact *via* both polar interactions and hydrogen bonding). For all three layered materials, the corresponding I_{sp} values (Table 1) were measured to be around 25 mJ/m^2 for ethylacetate and around 35 mJ/m^2 for 1-propanol. These I_{sp} values are roughly on the same order of magnitude as those found for conventional organic polymers and graphites, as determined by IGC.[50,51,57] Furthermore, their values approach those of the dispersive surface energy of MoS_2 and $MoSe_2$, implying that specific interactions in these materials play an important role during exfoliation. Simple addition of I_{sp} to γ_D yields a crude estimate for the total surface energy of the layered materials of around 75 mJ/m^2 (MoS_2 and $MoSe_2$) to around 120 mJ/m^2 ($MoTe_2$). Despite the obvious limitations of this estimate, it provides clear experimental evidence that the total surface energies of MoS_2, $MoSe_2$, and $MoTe_2$ are significantly lower than previously theoretically predicted,[39,48] with its numerical values probably lying between conventional organic polymers and clean graphitic surfaces.

In addition, in the cases of MoS_2 and $MoSe_2$, these surface energies are very similar to the values estimated from the solubility measurements shown in Figure 3. This similarity suggests that while surface energy is not an ideal solubility parameter for these layered compounds (due to the scatter observed in Figure 3), it can be used as a first-order approximation. We note that the measured surface energy of $MoTe_2$ is significantly higher than that indicated by Figure 3. There are a number of possible reasons for this discrepancy. It is possible that defects or impurities in the $MoTe_2$ powder introduce high-energy sites at the $MoTe_2$ surface, resulting in a pronounced bias of the IGC measurements (conducted at relatively low surface coverage) toward artificially high surface energy values. Alternatively, it is possible that the surface energy actually is high compared to the other compounds. In this scenario, the solubility data in Figure 3D may be misleading. As alluded to above, it is possible that these data represent the low energy tail of a peak which is centered at higher surface energies. In fact, we should note that we are limited by the solvents to which we have access. These typically have surface tensions <45 mJ/m^2 and so surface energies <75 mJ/m^2. Thus the position of this peak may be an artifact simply due to the limited range of available solvents.

Computer Modeling. We have used density functional theory (DFT) to calculate the surface energy of MoS_2. We calculated the difference between the energy of a slab of n layers and n times the energy per layer in bulk (obtained with a 24 layer supercell). This results in a surface energy of $E_S = E_n^{Slab} - n\varepsilon_{bulk})/2$, where E_n^{Slab} is the slab energy, n is the number of layers used to model the slab (in our model n = 19), and ε_{bulk} is the energy per layer in bulk. The converged surface energy was about 180 mJ/m^2.

Clearly, the calculated surface energy is more than a factor of 2 higher than that measured experimentally. At present, the sources of this discrepancy are not clear. For graphite, the DFT functional used compares well to calculations performed with advanced electronic structure methods.[58] However, a benchmark with

experiments is more difficult, as the experimental data contain a large degree of scatter.[58] It is therefore difficult to say whether or not the error may be simply attributed to the lack of accuracy of the functional or to the pseudopotential approximation. Notably, the DFT calculations describe the exfoliation of layered MoS_2 in vacuum, while experiments deal with a solvation problem, so that difference may arise simply because the present level of theory does not take into account effects associated with the solvent such as screening. Interestingly, our computational value is considerably lower than previous computational estimates of 260 and 284 mJ/m^2.[47,48]

Hansen Solubility Parameters. We noted above that when concentration is plotted *versus* surface energy, many samples have concentrations significantly lower than what would be expected from the envelope function for that surface energy. This phenomenology is ubiquitous and stems from the fact that surface energy is a rather crude solubility parameter.[25,33,34,45] To see why this is the case, we turn to another type of solubility parameter, the Hildebrand solubility parameter.[41]

In areas such as polymer physics,[59] it is very common to express the enthalpy of mixing *via* the Hildebrand solubility parameter, δ_T. Applying this framework to the dispersions under study here gives[34]

$$\frac{\Delta H_{Mix}}{V} \approx (\delta_{T,S} - \delta_{T,NS})^2 \phi \qquad (10)$$

where we assume the nanosheet volume fraction is low enough that we can write $(1 - \phi) \approx 1$. Inserting this expression in eq 3 gives[42]

$$C \propto \exp\left[-\frac{\bar{v}}{RT}(\delta_{T,S} - \delta_{T,NS})^2\right] \qquad (11)$$

This expression suggests that the dispersed nanosheet volume fraction scales as a Gaussian with solvent Hildebrand parameter and is consistent with standard solubility theory.[41] We plot A/l for MoS_2 dispersed in a range of solvents as a function of the solvent Hildebrand parameter $\delta_{T,S}$ in Figure 5A (the equivalent data for other solvents are plotted in Figure S4). We see a clear peak close to 22 MPa$^{1/2}$, bounded by a Gaussian envelope function. This result can be compared to similar plots for carbon nanotubes[33] and graphene[25] which show peaks centered at ~22 and ~21 MPa$^{1/2}$, respectively. However, like the surface energy data, there are many data points with concentrations lower than expected from the envelope function. The reason for this apparent discrepancy is that the Hildebrand parameter is equal to the square root of the cohesive energy density, and so eq 10 is a statement of the fact that the enthalpy is minimized when the total cohesive energy density of solvent and solute match. However, the total cohesive energy density actually consists of a number of terms, with those due to dispersion, dipole,

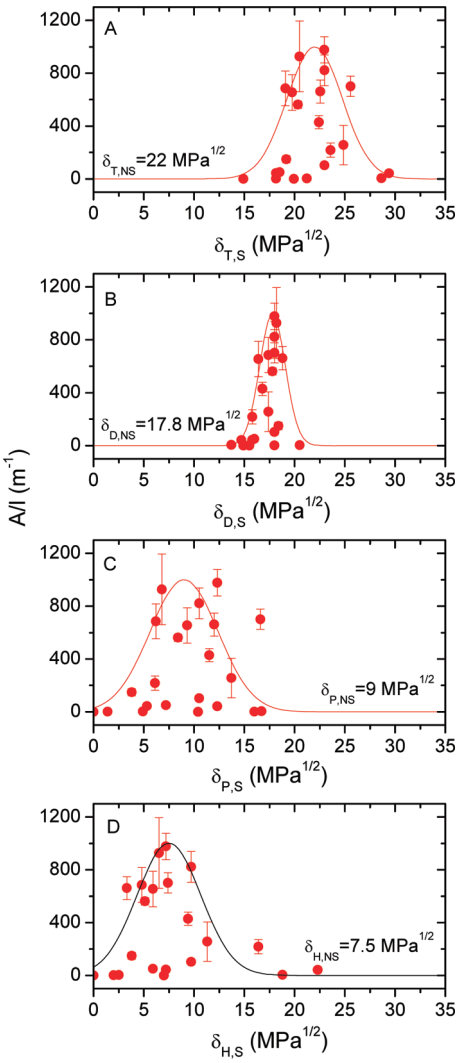

Figure 5. Absorbance per cell length (proportional to dispersed concentration) for MoS_2 dispersed in a range of solvents plotted as a function of Hildebrand and Hansen solubility parameters: (A) Hildebrand parameter, (B) Hansen's dispersive solubility parameter, (C) Hansen's polar solubility parameter, (D) Hansen's H-bonding solubility parameter. The lines represent Gaussian envelope functions.

and H-bonding interactions usually considered in solubility studies.[60] Hansen suggested that there are solubility parameters associated with each of these terms, the dispersive, polar, and H-bonding Hansen solubility parameters: δ_D, δ_P, and δ_H, respectively. These parameters can be related to the enthalpy of mixing by noting that

$$\frac{\Delta H_{Mix}}{V} \approx \frac{\chi}{\bar{v}_S} RT\phi \qquad (12)$$

where $\bar{v}_S$ is the solvent molar volume and χ is the Flory–Huggins parameter.[59,60] Within Hansen's framework, $\chi/\bar{v}_S$ is given by[60]

$$\frac{\chi}{\bar{v}_S} = [(\delta_{D,S} - \delta_{D,NS})^2 + (\delta_{P,S} - \delta_{P,NS})^2/4 + (\delta_{H,S} - \delta_{H,NS})^2/4]/RT \qquad (13)$$

We note that Hansen included factors of 1/4 in this expression with the justification that it lead to more accurate results.[60] Substituting into eq 3, we get

$$C \propto \exp\left[\frac{\bar{v}}{\bar{v}_S}\chi\right] = \exp\left[-\frac{\bar{v}}{RT}[(\delta_{D,S} - \delta_{D,NS})^2 + (\delta_{P,S} - \delta_{P,NS})^2/4 + (\delta_{H,S} - \delta_{H,NS})^2/4]\right] \quad (14)$$

This expression predicts that the concentration is maximized only when all three solubility parameters match for solvent and nanosheet. Analysis based on Hansen solubility parameter has been applied to dispersed nanomaterials such as carbon nanotubes[33,61,62] and graphene[25,63] in recent years.

We plot *A*/*l* for MoS_2 dispersed in a range of solvents as a function of the dispersive, polar, and H-bonding solvent Hansen parameters in Figure 5B–D (the equivalent data for the other materials are plotted in Figure S1). We see peaks in each case, centered at 17.8, 9, and 7.5 $MPa^{1/2}$ for $\delta_{D,S}$, $\delta_{P,S}$, and $\delta_{H,S}$, respectively. In each case, the data are bounded by a Gaussian envelope function. Similar results were obtained for the other materials. The centers and widths of all of the envelope functions are given in Table 2. It is clear from these data that $\delta_{D,NS}$, $\delta_{P,NS}$, and $\delta_{H,NS}$ are very similar to the values reported for graphene[25] ($\delta_{D,G} \approx 18$ $MPa^{1/2}$, $\delta_{P,G} \approx 9$ $MPa^{1/2}$, and $\delta_{H,G} \approx 8$ $MPa^{1/2}$) and carbon nanotubes[33] ($\delta_{D,NT} \approx 17.8$ $MPa^{1/2}$, $\delta_{P,NT} \approx 7-8$ $MPa^{1/2}$, and $\delta_{H,NT} \approx 7-8$ $MPa^{1/2}$), respectively. In addition, we note that the peak widths are significantly smaller for the dispersive graphs compared to the polar and H-bonding data. In fact, in the light of eq 14, Hansen's factor of 1/4 predicts that the polar and H-bonding peaks should be twice as broad as the dispersive peak. This relationship is in fact approximately the case as can be seen from Table 2, justifying Hansen's introduction of this factor for these materials at least.

We also note that, for all of the Hansen plots, there are still data points with concentration below the envelope function. However, this apparent deviation is to be expected. Equation 14 predicts that a given data point will only match the envelope function of one of the Hansen parameters only if the other two Hansen parameters of the solvent match that of the nanosheet perfectly. Thus, while Figure 5 is instructive, it does not definitively confirm that the data are described by eq 14. Better confirmation can be achieved now that we approximately know the values of $\delta_{D,NS}$, $\delta_{P,NS}$, and $\delta_{H,NS}$ for each nanosheet. With this information, we can calculate $\chi/\bar{v}_S$ for each nanosheet in each solvent using eq 13. If solubility theory can be used to describe the concentration of dispersed nanosheets, then eq 14 predicts that *A*/*l* should decrease exponentially with $\chi/\bar{v}_S$. Shown in Figure 6 are data for *A*/*l* *versus* $\chi/\bar{v}_S$ for each nanosheets type. While there is considerable scatter, it is apparent that the dispersed concentration does indeed decay exponentially with $\chi/\bar{v}_S$. This is strong evidence that solubility theory can be used to describe, at least qualitatively, dispersions of nanoscale objects such as nanosheets in solvents.

It is worth considering the limitations of solubility parameter analysis. There is no doubt that solubility parameters, including those of Hildebrand and Hansen and those based on surface energy, describe the results of studies such as these, at least to first order. In addition, they have excellent predictive abilities and have previously resulted in the discovery of many new

TABLE 2. Centers (δ) and Widths (fwhm) for All Hildebrand and Hansen Parameter Envelope Functions (Note That These Were Found Manually and Are Subject to Considerable Error)

	$\delta_{T,NS}$ ($MPa^{1/2}$)	$fwhm_T$ ($MPa^{1/2}$)	$\delta_{D,NS}$ ($MPa^{1/2}$)	$fwhm_D$ ($MPa^{1/2}$)	$\delta_{P,NS}$ ($MPa^{1/2}$)	$fwhm_P$ ($MPa^{1/2}$)	$\delta_{H,NS}$ ($MPa^{1/2}$)	$fwhm_H$ ($MPa^{1/2}$)
WS_2	21.5	4.5	18	3.3	8	6.5	7.5	5
MoS_2	22	6.5	17.8	3	9	8	7.5	7.5
$MoSe_2$	22.5	6.5	17.8	2.5	8.5	8	6.5	6
$MoTe_2$	21	5	17.8	3.5	8	6	6.5	4.5

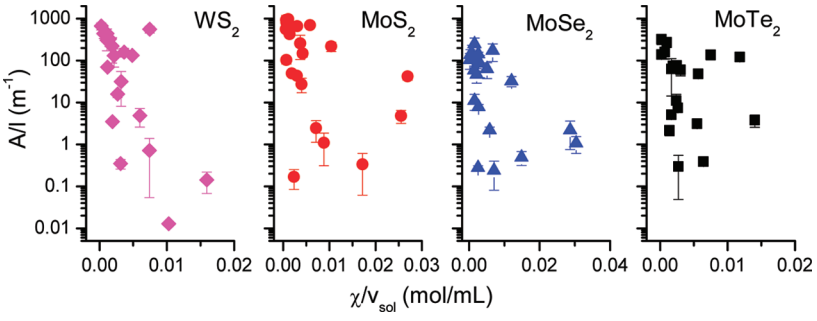

Figure 6. Absorbance per cell length (proportional to dispersed concentration) for all four TMDs dispersed in a range of solvents plotted as a function of Flory–Huggins parameter divided by solvent molar volume. Solubility theory predicts linear behavior.

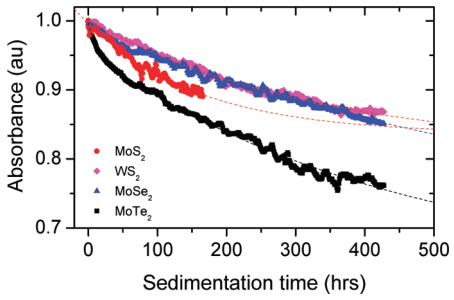

Figure 7. Sedimentation data for each of the four layered compounds dispersed in CHP. The dashed lines are fits to eq 15.

solvents for low-dimensional nanostructures.[23,25,34] However, it is extremely unlikely that solubility parameter models fully describe the solvation of nanostructures. Such scales are unable to capture any specific solvent−solute interactions that could aid or discourage solubility. As a result, the idea of matching energetic components of solvent with solute as described in equations such as 2 and 13 does not allow for a negative enthalpy of mixing, which may be important in such systems, where entropy of mixing is likely to be weak or unfavorable. Further investigation into specific interactions between low-dimensional nanostructures with solvents, using alternative solubility scales,[64] is warranted and will certainly enhance our understanding of these systems.

Stability of Dispersions. Finally, it is important to measure the stability of these dispersions. To do this, we chose CHP as a solvent which disperses all four materials reasonably well. These dispersions were prepared slightly differently from before. In each case, 100 mg of TMD powder was added to 10 mL of CHP. These mixtures were bath sonicated for 3 h. However, keeping in mind the concerns expressed above about bath sonication, they were then sonicated for 3 h using a point probe (VibraCell CVX, 750 W, 25% amplitude). Following this, they were then centrifuged using a Hettich Mikro 22R at 1500 rpm for 90 min. The top 6 mL was retained for analysis. To achieve the transparency required for sedimentation analysis, these dispersions were diluted by a factor of 20 with CHP (10 for WS_2).

We measured the stability of these dispersions using a home-built sedimentation apparatus.[65] This machine measures the absorbance of a dispersion as a function of time using a succession of laser pulses. For each dispersion, the measured absorbance is plotted as a function of sedimentation time in Figure 7. We see some sedimentation in all cases. However, after the first 100 h, over 90% of the dispersed material is retained in each case. Interestingly, the $MoTe_2$ sample appears considerably less stable than the other materials. Theoretical analysis shows that the concentration of a sedimentating phase as a function of time can be approximated by an exponential decay.[65] Thus, data such as that in Figure 7 can be fitted by the sum of a constant term (representing any stably dispersed material) and a number of exponential decays, each representing a specific type of sedimenting object. For example, previous work has shown that the sedimentation of flakes with two characteristic sizes can appear as two separate contributions to the sedimentation curve (each with a characteristic exponential decay).[66] We have found that the simplest expression consistent with all the data in Figure 7 is

$$A = A_0 + A_1 e^{-t/\tau_1} + A_2 e^{-t/\tau_2} \quad (15)$$

where A_0 represents the absorbance of the stable phase and A_1 and A_2 represent the initial absorbance of two sedimenting phases. However, we note that, for two of the samples, there is only one sedimenting phase (*i.e.*, $A_1 = 0$). Assuming that the different phases have similar absorption coefficients, then A_0, A_1, and A_2 represent the relative populations of each phase. The quantities τ_1 and τ_2 represent the sedimentation time constants of each sedimenting phase. This expression was fit to the data, as shown by the dashed lines in Figure 7. The fit constants are given in Table 3. In each case, the first sedimentating phase had extremely small values of A_1 (<5%), suggesting it represents a tiny minority of the material. In addition, the time constants associated with this phase are very short, <32 h, suggesting the sedimentation of relatively large objects.[65,66] Taken together, this suggests the objects sedimenting first to be unexfoliated crystallites which were not properly removed after centrifugation.[66] The second sedimentating phase had values of A_2 that shows it to represent between 16% and 36% of the initially dispersed material. In addition, it displays very long time constants (>161 h), suggesting that this phase consists of very small objects, possibly small flakes. It is unclear why a fraction of small flakes are unstable in these dispersions. However, most importantly, the stably dispersed phase has A_0 values between 62% and 84%, suggesting that the vast majority of dispersed, exfoliated material is stable over very long timeframes. This is, of course, important for any practical application of these dispersions.

TABLE 3. Sedimentation Fit Parameters Found from Fitting the Data in Figure 7 Using Equation 15

	A_0	A_1	τ_1 (h)	A_2	τ_2 (h)
MoS_2	0.84	0	NA	0.16	161
WS_2	0.81	0	NA	0.19	323
$MoSe_2$	0.62	0.02	32	0.36	977
$MoTe_2$	0.63	0.04	11	0.33	447

CONCLUSIONS

We have performed a comprehensive study into the dispersibility of WS_2, MoS_2, $MoSe_2$, and $MoTe_2$ in a range of solvents. For all four compounds, we have

shown that relatively high concentration dispersions are only obtained in solvents with surface energies close to 70 mJ/m^2 (that is surface tensions close to 40 mJ/m^2). Inverse gas chromatography measurements show MoS_2 and $MoSe_2$ to have surface energies close to 75 mJ/m^2. This agreement shows our results to be in agreement with solubility theory which predicts nanomaterials to be most effectively dispersed in solvents with matching surface energy. However, the dispersibility *versus* surface energy data show considerable scatter. We find that both Hildebrand and Hansen solubility parameters can be used to better describe the data. Within this framework, we find that all four materials have similar solubility parameters, and that the dispersed concentration tends to fall exponentially with Flory–Huggins parameter, as predicted by solution thermodynamics. We note that the development of IGC as an effective probe for nanomaterial surface chemistry offers considerable promise since other more routine chemical techniques are only limited by the nature of nanoparticulates; in principle, IGC can access a wide range of thermodynamic properties, as well as specific chemical interactions, and even phenomenology directly relevant to application.

The dispersion work is important as it answers a number of fundamental questions about solution-processing routes for two-dimensional materials. Most fundamentally, it shows that solution thermodynamics can be used as a framework to describe the dispersion of these materials. The surface energy can used as a solubility parameter for these materials, and importantly, dispersion studies suggest a value for the surface energy that is reasonably close to that measured independently for two of the compounds. In addition, this work suggests the surface energy to be similar for WS_2, MoS_2, and $MoSe_2$, with some uncertainty over $MoTe_2$. This uncertainty is partly due to the small number of solvents with surface tensions above 45 mJ/m^2, which makes it impossible to generate enough data to definitively determine the exact surface energy of the peak in concentration. However, these data ultimately show that similar solvents can be used to disperse and exfoliate each of these four layered materials. Indeed, this commonality suggests that the solvents used here represent a useful starting point for solvent exfoliation to other layered compounds. In addition, the availability of common solvents will facilitate the formation of composites of different layered compounds or of layered compounds with nanotubes or graphene. Finally, we find that Hansen solubility parameters probably provide a better description of the dependence of dispersibility on solvent. We find that each TMD has similar values of all three Hansen solubility parameters. Importantly, we find that the dispersed concentration decays exponentially with the Flory–Huggins parameter as predicted by solution thermodynamics.

METHODS

All materials were purchased in powder form and were all nominally >99% pure. For each material, the supplier and powder particle sizes were as follows: WS_2 (Sigma Aldrich, <2 μm), MoS_2 (Fluka, <2 μm), $MoSe_2$ (Cerac, <45 μm), and $MoTe_2$ (Cerac, ~10 μm). All solvents were >98% pure, purchased from Sigma Aldrich or Alfa Aesar, and used as received. Hygroscopic solvents were stored under 3 Å molecular sieves (Sigma-Aldrich, product number M9882). In all cases, dispersions were prepared by adding 75 mg of TMD powder to 10 mL of solvent in glass vials. For each TMD/solvent combination, three dispersions were prepared. Samples were batch sonicated using a Bandelin Sonorex RK1028H 28 L sonic bath (35 kHz, 300 W effective power) for a total of 400 min. As the bath is unlikely to have a uniform power distribution, it was divided into eight equally sized sections, and samples were cycled through each of the 8 sections remaining for 50 min in each. Following an established procedure,[23] the dispersions were then centrifuged at 1500 rpm (226*g*) for 90 min. The top 6 mL of each dispersion was then removed by pipet. These supernatants were placed in either 1 or 10 mm cuvettes and their absorbance spectra recorded using a Varian Cary 6000i in the wavelength range of 300–1200 nm. We report the mean (over three independent dispersions) absorbance per cell length (A/l) at the following fixed wavelengths (corresponding to the first visible peak in each spectrum): MoS_2 (670 nm), $MoSe_2$ (808 nm), $MoTe_2$ (701 nm), WS_2 (627 nm). The quoted error is half of the difference between minimum and maximum recorded A/l values. In this paper, we do not convert A/l to concentration because well-defined absorption coefficients are not available for each material in a wide range of solvents. This is because the nanoflakes in each dispersion may have slightly different sizes resulting in variations in the exponent describing the scattering background.[19,23] Such variations in background make it difficult to define an absorption coefficient which is intrinsic to each material.

Samples were prepared for TEM analysis by dropping 5 or 6 drops of dispersion onto holey carbon grids. TEM was performed using a JEOL JEM2100 with a LaB_6 gun operating at 200 kV. Thin films were prepared by filtration through porous membranes (Nitrocellulose from Millipore 0.025 μm). Raman measurements were performed with a 633 nm Horiba Jobin Yvon LabRAM- HR, while SEM analysis was performed with a Zeiss Ultra Plus.

Inverse gas chromatography measurements were carried out using a commercial instrument (Surface Measurement Systems Ltd., London, UK). The dispersive surface energies, γ_D, of MoS_2, $MoSe_2$, and $MoTe_2$ were determined *via* measurements of the retention of four nonpolar adsorbate vapors (*n*-hexane, *n*-heptane, *n*-octane, *n*-nonane), while the specific surface free energy ΔG_{sp} was measured using ethyl acetate and 1-propanol as polar probe vapors. An overview of the various adsorbates used (purchased from Sigma-Aldrich; HPLC grade) and some of their properties relevant to the analysis of the IGC data are given in the Supporting Information (Tables S2 and S3). All tests were performed using helium as a carrier gas and methane as an inert reference (both gases purchased from BOC; CP grade). Adsorbate vapors were generated from a liquid reservoir at a temperature of 30 °C. IGC samples were prepared by filling a small amount of powdered solid (between 150 and 250 mg) into a glass column of 3 mm inner diameter (purchased from SMS Ltd., London UK). The solid material was fixed in the column with plugs of silanized glass wool (purchased from SMS Ltd., London, UK) on both sides. The samples were preconditioned in the

column at 120 °C for 1 h before each measurement to ensure that surface contaminants were desorbed. The actual IGC measurements employed a column temperature of 40 °C and a flow rate of 10 mL/min. All IGC measurements were carried out at a constant adsorbate-to-adsorbent ratio of 0.15 (*i.e.*, at a hypothetical surface coverage of the solid surface by the adsorbate molecules of around 15%) in order to obtain comparable results despite the potential surface heterogeneity of the various chalcogenides.[51] The net retention volume, V_n, of an adsorbate is computed from its retention time, t_r, and the dead time, t_0, determined using methane as reference:[67]

$$V_n = (t_r - t_0)F\frac{j}{m}\frac{T}{273\ \mathrm{K}} \quad (16)$$

where F is the flow rate, T is the column temperature in Kelvin, m the solid sample mass, and j is the column pressure correction taking into account the pressure drop across the packed powder bed.

Surface energy calculations were made using DFT, specifically the newly developed nonlocal energy functional of Dion *et al.*,[68−70] as implemented in the plane-wave code Quantum-Espresso.[71] The implementation of the nonlocal correlation part of the total energy is based on the method of Roman-Perez and Soler.[72] Norm-conserving pseudopotentials are used for both Mo and S. The wave functions are expanded over a plane-wave basis set with a kinetic energy cutoff up to 100 Ryd. The Brillouin zone (BZ) integration of the hexagonal *P*63/*mmc* (6 atom−2 layers) cell for the MoS_2 bulk is sampled with a homogeneous $4 \times 4 \times 4$ Monkhorst-Pack mesh of k-points. This introduces an error smaller than 5×10^{-3} eV in the evaluation of band energy differences (*e.g.*, between the top and the bottom of valence band) and less than 1 mÅ in the evaluation of the in-plane lattice parameter. A minimization scheme is applied until all of the components of all forces are smaller than 0.003 eV/Å. The theoretical equilibrium lattice parameter $a = 3.099$ Å is obtained from the Murnaghan interpolation of the energy volume curves of fully optimized configurations, and it is in good agreement with the experimental value[73] of 3.13 Å, measured at 77 K. The unreconstructed MoS_2(100)1 × 1 surface is modeled in a slab geometries with 19 layers and a total number of 57 atoms. We fixed the in-plane lattice parameters to the *ab initio* equilibrium value of the bulk. A top and side view of the surface model for a two-layer surface is shown in the Supporting Information (Figure S1). To sample the BZ, a mesh of $4 \times 4 \times 1$ k-points was used.

Conflict of Interest: The authors declare no competing financial interest.

Acknowledgment. The authors thank Science Foundation Ireland for financial support through the Principle Investigator scheme, Grant Number 07/IN.1/I1772, as well as the European Research Council (grant − SEMANTICS). R.M. and M.S. thank EPSRC (EP/G007314/1) for support.

Supporting Information Available: Additional information on inverse gas chromatography and computation. Table of dispersion absorbance for all samples. This material is available free of charge *via* the Internet at http://pubs.acs.org.

REFERENCES AND NOTES

1. Geim, A. K. Graphene: Status and Prospects. *Science* **2009**, *324*, 1530–1534.
2. Geim, A. K.; Novoselov, K. S. The Rise of Graphene. *Nat. Mater.* **2007**, *6*, 183–191.
3. Huang, X.; Qi, X. Y.; Boey, F.; Zhang, H. Graphene-Based Composites. *Chem. Soc. Rev.* **2012**, *41*, 666–686.
4. Huang, X.; Yin, Z. Y.; Wu, S. X.; Qi, X. Y.; He, Q. Y.; Zhang, Q. C.; Yan, Q. Y.; Boey, F.; Zhang, H. Graphene-Based Materials: Synthesis, Characterization, Properties, and Applications. *Small* **2011**, *7*, 1876–1902.
5. Jiang, H. Chemical Preparation of Graphene-Based Nanomaterials and Their Applications in Chemical and Biological Sensors. *Small* **2011**, *7*, 2413–2427.
6. Lee, C.; Yan, H.; Brus, L. E.; Heinz, T. F.; Hone, J.; Ryu, S. Anomalous Lattice Vibrations of Single- and Few-Layer MoS_2. *ACS Nano* **2010**, *4*, 2695–2700.
7. Rao, C. N. R.; Nag, A. Inorganic Analogues of Graphene. *Eur. J. Inorg. Chem.* **2010**, 4244–4250.
8. Matte, H.; Gomathi, A.; Manna, A. K.; Late, D. J.; Datta, R.; Pati, S. K.; Rao, C. N. R. MoS_2 and WS_2 Analogues of Graphene. *Angew. Chem., Int. Ed.* **2010**, *49*, 4059–4062.
9. Yin, Z.; Li, H.; Li, H.; Jiang, L.; Shi, Y.; Sun, Y.; Lu, G.; Zhang, Q.; Chen, X.; Zhang, H. Single-Layer MoS_2 Phototransistors. *ACS Nano* **2011**, *6*, 74–80.
10. Li, H.; Yin, Z. Y.; He, Q. Y.; Huang, X.; Lu, G.; Fam, D. W. H.; Tok, A. I. Y.; Zhang, Q.; Zhang, H. Fabrication of Single- and Multilayer MoS_2 Film-Based Field-Effect Transistors for Sensing NO at Room Temperature. *Small* **2012**, *8*, 63–67.
11. Dean, C. R.; Young, A. F.; Meric, I.; Lee, C.; Wang, L.; Sorgenfrei, S.; Watanabe, K.; Taniguchi, T.; Kim, P.; Shepard, K. L.; *et al.* Boron Nitride Substrates for High-Quality Graphene Electronics. *Nat. Nanotechnol.* **2010**, *5*, 722–726.
12. Zeng, Z. Y.; Yin, Z. Y.; Huang, X.; Li, H.; He, Q. Y.; Lu, G.; Boey, F.; Zhang, H. Single-Layer Semiconducting Nanosheets: High-Yield Preparation and Device Fabrication. *Angew. Chem., Int. Ed.* **2011**, *50*, 11093–11097.
13. Ayari, A.; Cobas, E.; Ogundadegbe, O.; Fuhrer, M. S. Realization and Electrical Characterization of Ultrathin Crystals of Layered Transition-Metal Dichalcogenides. *J. Appl. Phys.* **2007**, *101*, 014507.
14. Novoselov, K. S.; Jiang, D.; Schedin, F.; Booth, T. J.; Khotkevich, V. V.; Morozov, S. V.; Geim, A. K. Two-Dimensional Atomic Crystals. *Proc. Natl. Acad. Sci. U.S.A.* **2005**, *102*, 10451–10453.
15. Radisavljevic, B.; Radenovic, A.; Brivio, J.; Giacometti, V.; Kis, A. Single-Layer MoS_2 Transistors. *Nat. Nanotechnol.* **2011**, *6*, 147–150.
16. Radisavljevic, B.; Whitwick, M. B.; Kis, A. Integrated Circuits and Logic Operations Based on Single-Layer MoS_2. *ACS Nano* **2011**, *5*, 9934–9938.
17. Wilson, J. A.; Yoffe, A. D. Transition Metal Dichalcogenides Discussion and Interpretation of Observed Optical, Electrical and Structural Properties. *Adv. Phys.* **1969**, *18*, 193–335.
18. Chang, K.; Chen, W. X. *In Situ* Synthesis of MoS_2/Graphene Nanosheet Composites with Extraordinarily High Electrochemical Performance for Lithium Ion Batteries. *Chem. Commun.* **2011**, *47*, 4252–4254.
19. Smith, R. J.; King, P. J.; Lotya, M.; Wirtz, C.; Khan, U.; De, S.; O'Neill, A.; Duesberg, G. S.; Grunlan, J. C.; Moriarty, G.; *et al.* Large-Scale Exfoliation of Inorganic Layered Compounds in Aqueous Surfactant Solutions. *Adv. Mater.* **2011**, *23*, 3944–3948.
20. Ruoff, R. Calling All Chemists. *Nat. Nanotechnol.* **2008**, *3*, 10–11.
21. Joensen, P.; Frindt, R. F.; Morrison, S. R. Single-Layer MoS_2. *Mater. Res. Bull.* **1986**, *21*, 457–461.
22. Sandoval, S. J.; Yang, D.; Frindt, R. F.; Irwin, J. C. Raman-Study and Lattice-Dynamics of Single Molecular Layers of MoS_2. *Phys. Rev. B* **1991**, *44*, 3955–3962.
23. Coleman, J. N.; Lotya, M.; O'Neill, A.; Bergin, S. D.; King, P. J.; Khan, U.; Young, K.; Gaucher, A.; De, S.; Smith, R. J.; *et al.* Two-Dimensional Nanosheets Produced by Liquid Exfoliation of Layered Materials. *Science* **2011**, *331*, 568–571.
24. Han, W. Q.; Wu, L. J.; Zhu, Y. M.; Watanabe, K.; Taniguchi, T. Structure of Chemically Derived Mono- and Few-Atomic-Layer Boron Nitride Sheets. *Appl. Phys. Lett.* **2008**, *93*, 223103.
25. Hernandez, Y.; Lotya, M.; Rickard, D.; Bergin, S. D.; Coleman, J. N. Measurement of Multicomponent Solubility Parameters for Graphene Facilitates Solvent Discovery. *Langmuir* **2010**, *26*, 3208–3213.
26. Lin, Y.; Williams, T. V.; Connell, J. W. Soluble, Exfoliated Hexagonal Boron Nitride Nanosheets. *J. Phys. Chem. Lett.* **2010**, *1*, 277–283.
27. Warner, J. H.; Rummeli, M. H.; Bachmatiuk, A.; Buchner, B. Atomic Resolution Imaging and Topography of Boron Nitride Sheets Produced by Chemical Exfoliation. *ACS Nano* **2010**, *4*, 1299–1304.

28. Zhi, C. Y.; Bando, Y.; Tang, C. C.; Kuwahara, H.; Golberg, D. Large-Scale Fabrication of Boron Nitride Nanosheets and Their Utilization in Polymeric Composites with Improved Thermal and Mechanical Properties. *Adv. Mater.* **2009**, *21*, 2889–2893.
29. Zhou, K.-G.; Mao, N.-N.; Wang, H.-X.; Peng, Y.; Zhang, H.-L. A Mixed-Solvent Strategy for Efficient Exfoliation of Inorganic Graphene Analogues. *Angew. Chem., Int. Ed.* **2011**, *50*, 10839–10842.
30. Lotya, M.; Hernandez, Y.; King, P. J.; Smith, R. J.; Nicolosi, V.; Karlsson, L. S.; Blighe, F. M.; De, S.; Wang, Z. M.; McGovern, I. T.; *et al.* Liquid Phase Production of Graphene by Exfoliation of Graphite in Surfactant/Water Solutions. *J. Am. Chem. Soc.* **2009**, *131*, 3611–3620.
31. Lotya, M.; King, P. J.; Khan, U.; De, S.; Coleman, J. N. High-Concentration, Surfactant-Stabilized Graphene Dispersions. *ACS Nano* **2010**, *4*, 3155–3162.
32. Smith, R. J.; Lotya, M.; Coleman, J. N. The Importance of Repulsive Potential Barriers for the Dispersion of Graphene Using Surfactants. *New J. Phys.* **2010**, *12*, 125008.
33. Bergin, S. D.; Sun, Z. Y.; Rickard, D.; Streich, P. V.; Hamilton, J. P.; Coleman, J. N. Multicomponent Solubility Parameters for Single-Walled Carbon Nanotube−Solvent Mixtures. *ACS Nano* **2009**, *3*, 2340–2350.
34. Bergin, S. D.; Nicolosi, V.; Streich, P. V.; Giordani, S.; Sun, Z. Y.; Windle, A. H.; Ryan, P.; Niraj, N. P. P.; Wang, Z. T. T.; Carpenter, L.; *et al.* Towards Solutions of Single-Walled Carbon Nanotubes in Common Solvents. *Adv. Mater.* **2008**, *20*, 1876–1881.
35. Bergin, S. D.; Sun, Z. Y.; Streich, P.; Hamilton, J.; Coleman, J. N. New Solvents for Nanotubes: Approaching the Dispersibility of Surfactants. *J. Phys. Chem. C* **2010**, *114*, 231–237.
36. Hernandez, Y.; Nicolosi, V.; Lotya, M.; Blighe, F. M.; Sun, Z. Y.; De, S.; McGovern, I. T.; Holland, B.; Byrne, M.; Gun'ko, Y. K.; *et al.* High-Yield Production of Graphene by Liquid-Phase Exfoliation of Graphite. *Nat. Nanotechnol.* **2008**, *3*, 563–568.
37. Khan, U.; O'Neill, A.; Lotya, M.; De, S.; Coleman, J. N. High-Concentration Solvent Exfoliation of Graphene. *Small* **2010**, *6*, 864–871.
38. McDevitt, N. T.; Zabinski, J. S.; Donley, M. S. The Use of Raman Scattering To Study Disorder in Pulsed Laser Deposited MoS_2 Films. *Thin Solid Films* **1994**, *240*, 76–81.
39. Sekine, T.; Nakashizu, T.; Toyoda, K.; Uchinokura, K.; Matsuura, E. Raman Scattering in Layered Compound 2H-WS2. *Solid State Commun.* **1980**, *35*, 371–373.
40. Sugai, S.; Ueda, T.; Murase, K. Raman Scattering in MoS_2, $MoSe_2$ and Alpha-$MoTe_2$ at High Pressures. *J. Physiol. (Paris)* **1981**, *42*, 320–322.
41. Hildebrand, J. H.; Prausnitz, J. M.; Scott, R. L. *Regular and Related Solutions*, 1st ed.; Van Nostrand Reinhold Company: New York, 1970; p 228.
42. Hughes, J. M.; Aherne, D.; Bergin, S. D.; Streich, P. V.; Hamilton, J. P.; Coleman, J. N. Using Solution Thermodynamics To Describe the Dispersion of Carbon Nanotubes in Organic Solvents. *Nanotechnology* **2011**Submitted.
43. Lyklema, J. The Surface Tension of Pure Liquids: Thermodynamic Components and Corresponding States. *Colloids Surf., A* **1999**, *156*, 413–421.
44. Tsierkezos, N. G.; Filippou, A. C. Thermodynamic Investigation of *N*,*N*-Dimethylformamide/Toluene Binary Mixtures in the Temperature Range from 278.15 to 293.15 K. *J. Chem. Thermodyn.* **2006**, *38*, 952–961.
45. Coleman, J. N. Liquid-Phase Exfoliation of Nanotubes and Graphene. *Adv. Funct. Mater.* **2009**, *19*, 3680–3695.
46. Israelachvili, J. *Intermolecular and Surface Forces*, 2nd ed.; Academic Press: New York, 1991.
47. Weiss, K.; Phillips, J. M. Calculated Specific Surface-Energy of Molybdenite (MoS_2). *Phys. Rev. B* **1976**, *14*, 5392–5395.
48. Fuhr, J. D.; Sofo, J. O.; Saul, A. Adsorption of Pd on MoS_2-(1000): *Ab Initio* Electronic-Structure Calculations. *Phys. Rev. B* **1999**, *60*, 8343–8347.
49. Schultz, J.; Lavielle, L.; Martin, C. The Role of the Interface in Carbon-Fiber Epoxy Composites. *J. Adhes.* **1987**, *23*, 45–60.
50. Papirer, E.; Brendle, E.; Ozil, F.; Balard, H. Comparison of the Surface Properties of Graphite, Carbon Black and Fullerene Samples, Measured by Inverse Gas Chromatography. *Carbon* **1999**, *37*, 1265–1274.
51. Menzel, R.; Lee, A.; Bismarck, A.; Shaffer, M. S. P. Inverse Gas Chromatography of As-Received and Modified Carbon Nanotubes. *Langmuir* **2009**, *25*, 8340–8348.
52. Wang, S.; Zhang, Y.; Abidi, N.; Cabrales, L. Wettability and Surface Free Energy of Graphene Films. *Langmuir* **2009**, *25*, 11078–11081.
53. Tagawa, M.; Ohmae, N.; Umeno, M.; Gotoh, K.; Yasukawa, A. Contact-Angle Hysteresis in Carbon-Fibers Studied by Wetting Force Measurements. *Colloid Polym. Sci.* **1989**, *267*, 702–706.
54. James, A. M.; Lord, M. P. *Macmillan's Chemical and Physical Data*; Macmillan: London, 1992.
55. Bjorkman, T.; Gulans, A.; Krasheninnikov, A. V.; Nieminen, R. M. Van Der Waals Bonding in Layered Compounds from Advanced First-Principles Calculations. *Phys. Rev. Lett.* **2012**Submitted.
56. Della Volpe, C.; Siboni, S. Some Reflections on Acid-Base Solid Surface Free Energy Theories. *J. Colloid Interface Sci.* **1997**, *195*, 121–136.
57. Diaz, E.; Ordonez, S.; Vega, A.; Coca, J. Evaluation of Adsorption Properties of Zeolites Using Inverse Gas Chromatography: Comparison with Immersion Calorimetry. *Thermochim. Acta* **2005**, *434*, 9–14.
58. Lebegue, S.; Harl, J.; Gould, T.; Angyan, J. G.; Kresse, G.; Dobson, J. F. Cohesive Properties and Asymptotics of the Dispersion Interaction in Graphite by the Random Phase Approximation. *Phys. Rev. Lett.* **2010**, *105*, 196401.
59. Rubinstein, M.; Colby, R. H. *Polymer Physics*, 1st ed.; Oxford University Press: Oxford, 2003; p 440.
60. Hansen, C. M. *Hansen Solubility Parameters - A User's Handbook*; CRC Press: Boca Raton, FL, 2007.
61. Detriche, S.; Zorzini, G.; Colomer, J. F.; Fonseca, A.; Nagy, J. B. Application of the Hansen Solubility Parameters Theory to Carbon Nanotubes. *J. Nanosci. Nanotechnol.* **2007**, *8*, 6082–6092.
62. Ham, H. T.; Choi, Y. S.; Chung, I. J. An Explanation of Dispersion States of Single-Walled Carbon Nanotubes in Solvents and Aqueous Surfactant Solutions Using Solubility Parameters. *J. Colloid Interface Sci.* **2005**, *286*, 216–223.
63. Li, F. H.; Bao, Y.; Chai, J.; Zhang, Q. X.; Han, D. X.; Niu, L. Synthesis and Application of Widely Soluble Graphene Sheets. *Langmuir* **2010**, *26*, 12314–12320.
64. Katritzky, A. R.; Fara, D. C.; Yang, H.; Taemm, K.; Tamm, T.; Karelson, M. Quantitative Measures of Solvent Polarity. *Chem. Inf.* **2004**, *35*, 175–198.
65. Nicolosi, V.; Vrbanic, D.; Mrzel, A.; McCauley, J.; O'Flaherty, S.; McGuinness, C.; Compagnini, G.; Mihailovic, D.; Blau, W. J.; Coleman, J. N. Solubility of $Mo_6S_{4.5}I_{4.5}$ Nanowires in Common Solvents: A Sedimentation Study. *J. Phys. Chem. B* **2005**, *109*, 7124–7133.
66. O'Neill, A.; Khan, U.; Nirmalraj, P. N.; Boland, J.; Coleman, J. N. Graphene Dispersion and Exfoliation in Low Boiling Point Solvents. *J. Phys. Chem. C* **2011**, *115*, 5422–5428.
67. Condor, J. L.; Young, C. L. *Physicochemical Measurements by Gas Chromatography*; John Wiley and Sons: New York, 1979.
68. Dion, M.; Rydberg, H.; Schroder, E.; Langreth, D. C.; Lundqvist, B. I. Van Der Waals Density Functional for General Geometries. *Phys. Rev. Lett.* **2004**, *92*, 246401.
69. Langreth, D. C.; Lundqvist, B. I.; Chakarova-Kack, S. D.; Cooper, V. R.; Dion, M.; Hyldgaard, P.; Kelkkanen, A.; Kleis, J.; Kong, L. Z.; Li, S.; *et al.* A Density Functional for Sparse Matter. *J. Phys.: Condens. Matter* **2009**, *21*, 084203.
70. Thonhauser, T.; Cooper, V. R.; Li, S.; Puzder, A.; Hyldgaard, P.; Langreth, D. C. Van Der Waals Density Functional: Self-Consistent Potential and the Nature of the Van Der Waals Bond. *Phys. Rev. B* **2007**, *76*, 125112.
71. www.pwscf.org.
72. Roman-Perez, G.; Soler, J. M. Efficient Implementation of a Van Der Waals Density Functional: Application to Double-Wall Carbon Nanotubes. *Phys. Rev. Lett.* **2009**, *103*, 096102.
73. Young, P. A. Lattice Parameter Measurements on Molybdenum Disulphide. *J. Phys. D: Appl. Phys.* **1968**, *1*, 936–939.

74. Diaz, E.; Ordonez, S.; Vega, A. Adsorption of Volatile Organic Compounds onto Carbon Nanotubes, Carbon Nanofibers, and High-Surface-Area Graphites. *J. Colloid Interface Sci.* **2007**, *305*, 7–16.
75. Menzel, R.; Bismarck, A.; Shaffer, M. S. P. Deconvolution of the Structural and Chemical Surface Properties of Carbon Nanotubes by Inverse Gas Chromatography. *Carbon* 2012, published online, http://dx.doi.org/10.1016/j.carbon.2012.02.094.